ELSEVIER

Engineering Analysis with Boundary Elements 31 (2007) 343–360

ENGINEERING ANALYSIS with BOUNDARY ELEMENTS

www.elsevier.com/locate/enganabound

# Solution of identification inverse problems in elastodynamics using semi-analytical sensitivity computation

Guillermo Rus, Rafael Gallego*

*Department of Structural Mechanics, University of Granada, Spain*

Received 14 February 2006; accepted 4 October 2006
Available online 20 November 2006

**Abstract**

The purpose of this work is to study a class of inverse problems that arises in solid mechanics areas such as quantitative non-destructive testing (QNDT) or shape optimization. The technique is based on the boundary integral equations (BIEs) used in the classical boundary element method (BEM), which are differentiated semi-analytically with respect to variations of the boundary geometry and used in an iterative search algorithm. The extension of this strategy is presented here for the case of elasticity in dynamics using the displacement or singular BIE, which allows to apply this strategy to QNDT problems based on vibrations or ultrasonics.

The central point is the evaluation of the capability of solving numerically a QNDT problem such as the location and characterization of cavity and inclusion-type defects by measuring the dynamic response at an accessible boundary of the specimen. To test this capability, comprehensive convergence tests are made for the badness of the initial guess, the amount of supplied measurements, and simulated errors on measurements, geometry, elastic constants and frequency.


*PACS:* 43.40.L; 81.70

*Keywords:* Sensitivity; Identification inverse problem (IIP); Optimization algorithms; Quantitative non-destructive evaluation (QNDE); Boundary element method (BEM); Boundary integral equations (BIEs); Parametrization

## 1. Introduction

A direct problem can be stated as the calculation of the response (for instance, certain displacements $u$ and tractions $q$) in a specific body defined by its geometry $\Omega$, mechanical properties ($k$), physical model (operator $L$) and boundary conditions (some known values of $u$ and $q$). In opposition to this, an *inverse problem* (IP) is one in which part of the information above is unknown. If a generic direct problem is defined as

$$L(k)u = q \quad \text{on } \Omega \tag{1}$$

different IPs can be stated depending on the nature of the unknown (see the classification by Kubo [1]). To find the missing information, additional data from the response have to be provided, besides the boundary conditions. This additional data $u^{ex}$ or $q^{ex}$ are obtained experimentally at some points of the domain or its boundary $\Gamma$.

This paper is aimed at the solution of the so-called *identification inverse problem* (IIP), where the unknown is a part of the domain. This problem arises in many branches of science and engineering, but the interest of the authors is mainly the development of computerized non-destructive techniques, aimed at the detection of flaws inside a unreachable part of a mechanical or structural element.

A general IP can be written alternatively,

(1) as the solution of a set of implicit nonlinear equations called *observation equations*, that relate some properly chosen *design variables* $P_g$ and the experimental

*Corresponding author.
*E-mail addresses:* grus@ugr.es (G. Rus), gallego@ugr.es (R. Gallego).

0955-7997/$ - see front matter © 2006 Elsevier Ltd. All rights reserved.
doi:10.1016/j.enganabound.2006.10.001

data, $v^{ex}$,

$F(P_g) = v^{ex}$

(2) or as an *optimization problem*, where the residual of the former set of equations is minimized,

$$\min_{P_g} \tfrac{1}{2}\|F(P_g) - v^{ex}\|^2.$$

In both cases, the most time-efficient solution algorithms use sensitivity information (gradient), which should be computed accurately and efficiently.

To perform this computation, besides the obvious but time-consuming finite differences approach, two analytical tools are available: direct differentiation method and adjoint state approach. The first one was used by Nishimura et al. [2], Meric et al. [3], Aithal and Saigal [4], Mellings and Aliabadi [5], Lee and Kwak [6] and Rus and Gallego [7]. It is based on the direct differentiation of the equations with respect to the geometrical parameters which define the unknown flaw. Mukherjee et al. [8–10] develop the direct differentiation formulation for the indirect boundary contour method for 3D static elasticity, first for boundary and then for internal points, and obtain moderately good convergence.

On the other hand Bonnet et al. [11–13] applied the adjoint state approach to the boundary integral equations (BIEs) to find the sensitivity to geometry variation of a cavity in bidimensional elasticity and, later, in elastodynamics [14,15]. The same approach was used by Burczynski et al. [16] and compared to the direct differentiation.

The IP of locating a cavity using elastodynamic measurements has been solved using the adjoint state approach for the geometrical sensitivity and the Broyden–Fletcher–Goldfarb–Shanno (BFGS) nonlinear solution method for the minimization of the quadratic cost functional by Guzina et al. [17] for the case of 3D elastodynamics, attaining convergence for a single elipsoidal cavity.

In this paper, the *sensitivity boundary integral equation* or *variation boundary integral equation* developed by Rus [18] is used to supply the necessary geometrical gradient for the search algorithm used for solving a complete IIP. This method for determining the geometrical sensitivity is preferred above the adjoint state approach due to the much lower requirements on discretization density, which extends considerably the time of convergence. The accuracy and rate of convergence of the resulting algorithm is exhaustively checked. The *sensitivity boundary integral equation* provides the sensitivity of displacements and tractions in an harmonic elastodynamics state due to *changes in the geometry of an internal cavity or inclusion*. This equation is obtained by a series expansion and a linearization, following a procedure first proposed by Tanaka et al. [19] for potential problems, and Aithal et al. [4] for static elasticity. In these papers some important terms where missing and a first corrected formulation was presented for potential problems by Gallego et al. [20] in 1998 and by Rus et al. [21] in 2005. The latter paper addresses the detailed description of the present semi-analytical method for sensitivity computation as well as a comparative study between the performance obtained by the semi-analytical method and by finite differences. The final equation should be equivalent to that obtained by Bonnet et al. [11] using material differentiation, but no attempt has been made yet to prove this.

## 2. Solution of the IP

Given the definition of IP as the characterization of the output data, which in the IIP are the parameters that define the location and shape of defects inside a specimen, using as input data the mechanical model of the specimen as well as a set of measurements or responses of the faulty specimen measured at an accessible boundary, the general scheme in Fig. 1 for the solution of IP can be established based on the search of the correct parameters that minimize the discrepancy between computed and measured responses.

The first point to be addressed is the provision of the gradient of the cost functional or the residuals, which is done by a semi-analytical sensitivity of the BIE that governs the elasticity model of the specimen. The following point describes the computational solution of the equations. Next, the parametrization is addressed as the procedure to characterize the defects, being a critical point for the definition and robustness of the output of the problem. The last theoretical point regards the search and minimization algorithm.

Several tests are carried out. First the partial results of the sensitivity computation. Then, the convergence of the search given a complete IIP is verified.

## 3. Sensitivity BIE

The solution of the ensuing *sensitivity boundary integral equation* (or $\delta u$BIE) will provide the values of the sensitivities of displacements $\delta\mathbf{u}$ and tractions $\delta\mathbf{q}$ on the boundary with respect to a change of the geometry $\delta\mathbf{x}$. The sensitivity of a generic cost or objective functional $\mathscr{J}$ defined as

$$\mathscr{J}(\Gamma_c) = \int_{\Gamma_q} \varphi_u(\mathbf{u})\,\mathrm{d}\Gamma + \int_{\Gamma_u} \varphi_q(\mathbf{q})\,\mathrm{d}\Gamma + \int_{\Gamma_f} \psi(\mathbf{x})\,\mathrm{d}\Gamma \tag{2}$$

which can be computed by applying the chain rule,

$$\delta\mathscr{J}(\Gamma_c) = \int_{\Gamma_q} \frac{\partial\varphi_u}{\partial\mathbf{u}}\delta\mathbf{u}\,\mathrm{d}\Gamma + \int_{\Gamma_u} \frac{\partial\varphi_q}{\partial\mathbf{q}}\delta\mathbf{q}\,\mathrm{d}\Gamma + \int_{\Gamma_f} \frac{\partial\psi}{\partial\mathbf{x}}\delta\mathbf{x}\,\mathrm{d}\Gamma \tag{3}$$

assuming that the fractions of the boundary $\Gamma_q$, $\Gamma_u$ and $\Gamma_f$ are accessible, and therefore fixed.

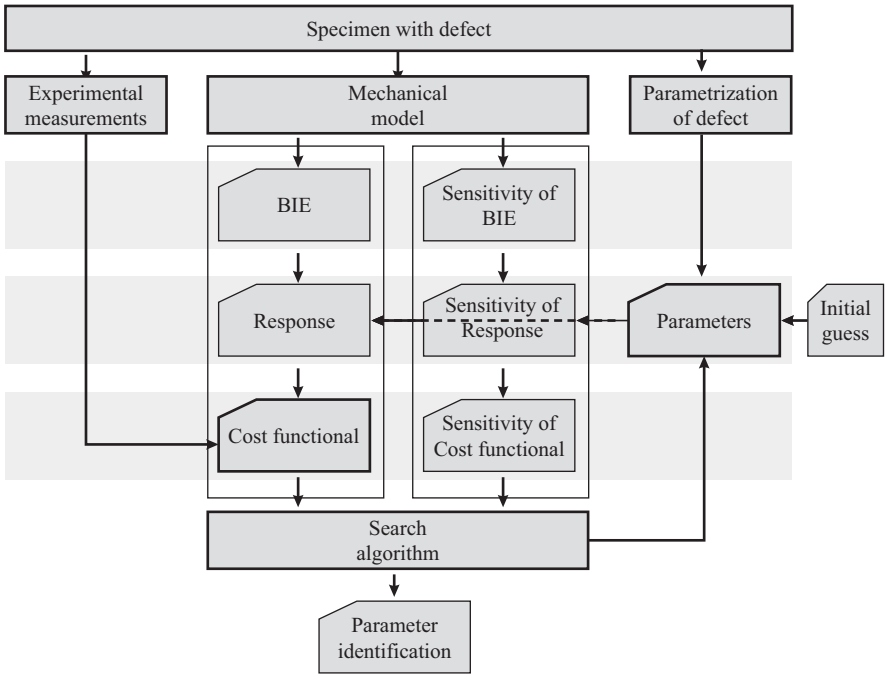


Fig. 1. General scheme of the solution of inverse problems by search of parameters to minimize the measurement discrepancy.

The goal becomes therefore to calculate the variation of the boundary integral equation *u*BIE with respect to changes in the geometry of the boundary $\Gamma$. The geometrical change is described as an infinitesimal field $\delta\mathbf{x}(\mathbf{x}) = \delta x_i(\mathbf{x})$, such that the coordinates of a point $\mathbf{x} = x_i$ will change after the perturbation to $\tilde{x}_i = x_i + \delta x_i(\mathbf{x})$. Note that $\mathbf{x}$ is a generic point on the boundary or/and *inside* $\Omega$. This fact, among others, was overlooked in the cited previous works.

In a domain $\Omega$ bounded by $\Gamma$, the displacement integral equation (or *u*BIE, see [22]) can be written as

$$c_k^i(\mathbf{y})u_k(\mathbf{y}) + \int_\Gamma [q_k^i(\mathbf{x};\mathbf{y})u_k(\mathbf{x}) - u_k^i(\mathbf{x};\mathbf{y})q_k(\mathbf{x})]\,\mathrm{d}\Gamma(\mathbf{x}) = 0, \tag{4}$$

where $u_k(\mathbf{x})$ is the $k$th component of the displacement vector in the actual state at the *observation point* $\mathbf{x} = x_j$; $q_k(\mathbf{x}) = \sigma_{jk}(\mathbf{x})n_j(\mathbf{x})$ the traction in the actual state at point $\mathbf{x}$. $\sigma_{jk}(\mathbf{x})$ is the stress tensor and $n_j$ the outward normal. $u_k^i(\mathbf{x};\mathbf{y})$ is the $k$th component of the displacement vector at the observation point $\mathbf{x}$ due to a point load applied in direction $i$ at the *collocation point* $\mathbf{y}$. The expression for this fundamental solution for two-dimensional harmonic elastodynamics is readily available from the literature (for example [18]). $q_k^i(\mathbf{x};\mathbf{y}) = \sigma_{lk}^i(\mathbf{x};\mathbf{y})n_l(\mathbf{x})$ is the traction of the fundamental solution and $c_k^i$ the free term whose value depends on the position of the collocation point. Thus, $c_k^i(\mathbf{y}) = \delta_k^i$ (Kroenecker delta) if $\mathbf{y} \in \Omega$; $c_k^i(\mathbf{y})$ depends on the geometry of the boundary at $\mathbf{y}$ if $\mathbf{y} \in \Gamma$, and is such that $c_k^i(\mathbf{y}) = \frac{1}{2}\delta_k^i$ when the boundary is smooth (continuous normal) at $\mathbf{y}$; $c_k^i(\mathbf{y}) = 0$ otherwise.

The derivation of the proposed sensitivity BIE follows these steps:

(1) The displacement integral equation is established both for the actual domain, and for the perturbed one, with the observation point at the interior of the domain (i.e. $\mathbf{y} \in \Omega$ but $\mathbf{y} \notin \Gamma$).
(2) The variables in the last one are expanded as series in terms of the infinitesimal perturbation.
(3) Terms higher than linear are neglected and the integral for the actual domain is subtracted.
(4) The ensuing integral equation is taken to the boundary by a careful limiting process as done in the standard boundary integral method.

### 3.1. Variation of the integral equation

Consider Eq. (4) for a domain point $\mathbf{y}$, i.e., one *within* the body $\Omega$.

$$u_i(\mathbf{y}) + \int_\Gamma [q_k^i(\mathbf{x};\mathbf{y})u_k(\mathbf{x}) - u_k^i(\mathbf{x};\mathbf{y})q_k(\mathbf{x})]\,\mathrm{d}\Gamma(\mathbf{x}) = 0. \tag{5}$$

The displacements and tractions will change to $\tilde{u}_i(\tilde{\mathbf{x}})$ and $\tilde{q}_i(\tilde{\mathbf{x}})$ when the geometry is perturbed to $\tilde{\Omega}$. We now define the *variation* or *sensitivities of displacements* and *tractions* $\delta u_i$ and $\delta q_i$ from

$$\tilde{u}_i(\tilde{\mathbf{x}}) = u_i(\mathbf{x}) + \delta u_i(\mathbf{x}), \tag{6}$$

$$\tilde{q}_i(\tilde{\mathbf{x}}) = q_i(\mathbf{x}) + \delta q_i(\mathbf{x}). \tag{7}$$

Note that these variations are *material*, in the sense that they include the change due to the modification of the

geometry ($\Omega$ to $\tilde{\Omega}$), as well as that of the change in the point of computation ($\mathbf{x}$ to $\tilde{\mathbf{x}}$).

To find the equations that these variations fulfill, the integral equation is written for the perturbed domain,

$$\tilde{u}_i(\tilde{\mathbf{y}}) + \int_{\tilde{\Gamma}} [q_k^i(\tilde{\mathbf{x}};\tilde{\mathbf{y}})\tilde{u}_k(\tilde{\mathbf{x}}) - u_k^i(\tilde{\mathbf{x}};\tilde{\mathbf{y}})\tilde{q}_k(\tilde{\mathbf{x}})]\,\mathrm{d}\tilde{\Gamma}(\tilde{\mathbf{x}}) = 0. \tag{8}$$

The kernels in this equation are computed at perturbed points. It is simple to relate them with the kernels at the actual points by a Taylor expansion:

$$\begin{aligned} u_k^i(\tilde{\mathbf{x}};\tilde{\mathbf{y}}) &= u_k^i(\mathbf{x};\mathbf{y}) + \frac{\partial u_k^i}{\partial x_m}\delta x_m + \frac{\partial u_k^i}{\partial y_m}\delta y_m + \text{h.o.t.} \\ &= u_k^i(\mathbf{x};\mathbf{y}) + u_{k,m}^i \delta r_m + \text{h.o.t.} \end{aligned} \tag{9}$$

accounting for the radial nature of the kernels, where the comma stands for derivation with respect to the coordinates of the observation point $\mathbf{x}$, and $\delta r_m = \delta x_m - \delta y_m$, and where h.o.t. stands for *higher order terms*.

For the kernel $q_k^i(\tilde{\mathbf{x}};\tilde{\mathbf{y}})$ the variation of the normal and of the length of boundary has to be taken into account as shown in the Appendix. Since $q_k^i(\tilde{\mathbf{x}};\tilde{\mathbf{y}}) = \tilde{\sigma}_{jk}^i(\tilde{\mathbf{x}};\tilde{\mathbf{y}})\tilde{n}_j(\tilde{\mathbf{x}})$, a similar procedure as above yields,

$$\begin{aligned} q_k^i(\tilde{\mathbf{x}};\tilde{\mathbf{y}}) \simeq\ & q_k^i(\mathbf{x};\mathbf{y}) + \sigma_{jk}^i(\mathbf{x};\mathbf{y})\delta n_j(\mathbf{x}) \\ & + \sigma_{jk,m}^i(\mathbf{x};\mathbf{y})\delta r_m n_j(\mathbf{x}) + \text{h.o.t.} \end{aligned} \tag{10}$$

Finally, the integral of any function $F$ along the perturbed domain can be related to the actual domain by

$$\int_{\tilde{\Gamma}} F\,\mathrm{d}\tilde{\Gamma} = \int_{\Gamma} F(1+\delta S)\,\mathrm{d}\Gamma + \text{h.o.t.} \tag{11}$$

where $\delta n_j$ and $\delta S$ are given by the formulas in the Appendix.

Collecting all the expressions above, substituting in the integral Eq. (8), subtracting Eq. (5), and neglecting terms higher than linear, the following integral equation is obtained:

$$\begin{aligned} &\delta u_i(\mathbf{y}) + \int_{\Gamma} [q_k^i(\mathbf{x};\mathbf{y})\delta u_k(\mathbf{x}) - u_k^i(\mathbf{x};\mathbf{y})\delta q_k(\mathbf{x})]\,\mathrm{d}\Gamma(\mathbf{x}) \\ &\quad = \int_{\Gamma} \{[u_{k,m}^i(\mathbf{x};\mathbf{y})q_k(\mathbf{x}) - \sigma_{jk,m}^i(\mathbf{x};\mathbf{y})n_j(\mathbf{x})u_k(\mathbf{x})]\delta r_m \\ &\qquad + [u_k^i(\mathbf{x};\mathbf{y})q_k(\mathbf{x}) - q_k^i(\mathbf{x};\mathbf{y})u_k(\mathbf{x})]\delta S(\mathbf{x}) \\ &\qquad - \sigma_{jk}^i(\mathbf{x};\mathbf{y})u_k(\mathbf{x})\delta n_j(\mathbf{x})\}\,\mathrm{d}\Gamma(\mathbf{x}). \end{aligned} \tag{12}$$

This integral equation relates the variation ($\delta\mathbf{x}$ and $\delta r_m$) of a domain point $\mathbf{x}$ with the variation of displacements and tractions ($\delta u_k$ and $\delta q_k$) at the boundary points, and the variation of the geometry of the boundary ($\delta n_j$ and $\delta S$).

The main advantage is that the field can be manipulated before defining any parametrization. This allows to define and implement the main sensitivity calculation with complete generality with respect to the choice of parametrization. In particular, the variation equation will only depend explicitly on the terms $\delta x_i$ and $\partial\delta x_i/\partial x_m$.

### 3.2. Limit to the boundary

The integral equation obtained in the previous section would be useful to compute sensitivities at internal points, but its *boundary* counterpart will provide the relationship between the sensitivities of displacements and tractions along the boundary *only* and the variation of the geometry.

In order to perform the limit, a point $\mathbf{y}$ at the boundary is considered, and the actual boundary is distorted (see [22]), which allows the usual decomposition of the boundary integral of any integrand $F$,

$$\int_{\Gamma} F\,\mathrm{d}\Gamma \to \int_{\Gamma-\Gamma_\varepsilon} F\,\mathrm{d}\Gamma + \int_{S_\varepsilon} F\,\mathrm{d}\Gamma \tag{13}$$

and the limit to the boundary of each term in Eq. (12) can be computed. The first integral converges in all cases, while the second yields a free or a null term [22]. Since the kernel is singular, to yield a finite integrand the source in the integrands have to be expanded to the proper order. Provided the continuity and derivability conditions in Table 1 are fulfilled, as proved by Rus [18,21], the *variation boundary integral equation* for the displacements (or $\delta u$BIE) is finally derived, which has the following expression for a smooth boundary collocation point:

$$\begin{aligned} &\frac{1}{2}\delta u_i(\mathbf{y}) + \int_{\Gamma} [q_k^i(\mathbf{x};\mathbf{y})\delta u_k(\mathbf{x}) - u_k^i(\mathbf{x};\mathbf{y})\delta q_k(\mathbf{x})]\,\mathrm{d}\Gamma(\mathbf{x}) \\ &\quad = \int_{\Gamma} \{[u_{k,m}^i(\mathbf{x};\mathbf{y})q_k(\mathbf{x}) - \sigma_{jk,m}^i(\mathbf{x};\mathbf{y})n_j(\mathbf{x})u_k(\mathbf{x})]\delta r_m \\ &\qquad + [u_k^i(\mathbf{x};\mathbf{y})q_k(\mathbf{x}) - q_k^i(\mathbf{x};\mathbf{y})u_k(\mathbf{x})]\delta S(\mathbf{x}) \\ &\qquad - \sigma_{jk}^i(\mathbf{x};\mathbf{y})u_k(\mathbf{x})\delta n_j(\mathbf{x})\}\,\mathrm{d}\Gamma(\mathbf{x}). \end{aligned} \tag{14}$$

### 3.3. Numerical evaluation

Standard boundary element techniques are employed to solve the $\delta u$BIE. The boundary is divided into a number of elements, and within each one the geometry, displacements, tractions and their variations are interpolated quadrati-

Table 1
Continuity requirements for each variable at the collocation point

| Variable | In $u$BIE | In $\delta u$BIE |
|---|---|---|
| $u_k$ | $C^{0,\alpha}$ | $C^{0,\alpha}$ |
| $q_k$ | Bounded | Bounded |
| $\sigma_{kl}$ | – | $C^{0,\alpha}$ |
| $\delta x_l$ | – | $C^{1,\alpha}$ |
| $\delta u_l$ | – | $C^{0,\alpha}$ |
| $\delta q_l$ | – | $C^{0,\alpha}$ |
| $\delta\sigma_{kl}$ | – | – |

–, means no conditions to fulfill and $C^{1,\alpha}$, means the Hölder condition, with $0 \leqslant \alpha < 1$. This implies that if $u_j \in C^{1,\alpha}$, then $u_j(\mathbf{x}) = u_j(\boldsymbol{\xi}) + u_{j,h}(\boldsymbol{\xi})(x_h - \xi_h) + O(r^{1+\alpha})$.

cally, where $\phi_n$ are standard quadratic base functions:

$$\mathbf{x} = \sum_{n=1}^{3} \phi_n \mathbf{x}^n, \quad \mathbf{u} = \sum_{n=1}^{3} \phi_n \mathbf{u}^n, \quad \mathbf{q} = \sum_{n=1}^{3} \phi_n \mathbf{q}^n,$$

$$\delta\mathbf{u} = \sum_{n=1}^{3} \phi_n \mathbf{u}^n, \quad \delta\mathbf{q} = \sum_{n=1}^{3} \phi_n \mathbf{q}^n.$$

Using these standard elements, the continuity conditions required in Table 1 are fulfilled. These results show that the collocation points for the $\delta u$BIE can be placed at the standard locations. Nevertheless, to simplify the computation, at corners, multiple collocation inside the adjacent elements are performed in the numerical tests.

## 4. Parametrization

In an IP, information such as the size and orientation of defects is sought based on the known forward problem (also known as direct problem). Finding such information is possible by first introducing some a priori information and setting the scope by means of a proper parametrization. This procedure is usually called regularization.

A simple strategy to characterize the system using a set of parameters ($P_g$) with a reduced number of variables ($g$). Choosing parameters is a critical step influencing the convergence, the sensitivity of the result and the decoupling of their dependence from the measurements.

The variation of the geometry during a step in the iterative inverse solution is represented by a so-called parametrization, which stands for a representation of the geometrical definition by a finite set of values. A generic and exact representation would need an infinite number of parameters. When the problem is discretized for the sake of solving it numerically, the geometry is then defined by some nodal coordinates. Taking as parameters each of those nodal coordinates, would yield the complete parametrization of this geometry, involving a finite but large number of data.

Many IPs are ill-posed: solutions may not exist, there may exist multiple solutions, they could be unstable and non-converging. The used iterative numerical methods for highly nonlinear and ill-conditioned equations they deal with are never guaranteed to converge, but the "probability" of convergence highly depend on the number of parameters to search. This ill-conditioning is rooted in the physical meaning of the problem, so this difficulty cannot be avoided by purely mathematical manipulations. Instead, some physical pieces of a priori information have to be provided, and this is called regularization. A drastic regularization is provided by a correct choice of parametrization, consisting on reducing the number of parameters by expressing the geometry by a fewer number of data.

### 4.1. Geometry variation field

The variation of the geometry $\delta\mathbf{x}$ previously defined is modelled as

$$\delta\mathbf{x} = \Theta_{ig}(\mathbf{x}, \delta P_g), \tag{15}$$

where $P_g$ represents a finite set of parameters that characterize *the variation of the geometry*, and $\Theta_{ig}$ is a parametrization matrix. A more advanced concept is adopted, which was first put forward by Gallego and Suárez [23]. It consists in defining directly the modification field instead of the geometry, after taking advantage of the fact that no parameterization of the geometry of the boundary is needed, but only of its variation. This means applying a deformation field to some initial geometry (as complicated as you want) that is capable of moving it until any possible solution. Now, it is this field which is defined by a set of parameters (for example a linear deformation field that in 2D is defined by six parameters, which has been used by Gallego et al. [7,24]). This field is only non-zero for the sought part of the geometry (the flaw or the zone to be optimized). One reason to support this choice of deformation field is the congruence of the sense of the derivative of the field, not only on the boundary but in its vicinity. Another reason is that a field can be applied to any geometry without a change of parametrization.

At a certain step $k$ in the iterative optimization procedure, there are two options in the definition of the parametrization matrix,

*Incremental parametrization*: Using the observation equation approach, in which the only information used for a step $k$ is the setup in step $k-1$, one may apply to the geometry $k-1$ a parameter set that will only last one iteration, and that will start and be applied to the geometry $k-1$:

$$x_i^k = x_i^{k-1} + \delta x_i^k(\mathbf{x}^{k-1}),$$

$$\delta x_i^k = \Theta_{ig}(\mathbf{x}^{k-1})\delta P_g.$$

*Global parametrization*: If the iterative method is more complicated one may need more information than just the last step. Therefore one may not use a one step parameter as before, but some history. It is possible to store artificially the necessary information, but there is a conceptually clearer procedure, which is to use a parameter that evolves throughout the iterative method. This parameter will be calculated from the initial geometry 0. This allows the parameter to be treated independently, as a black box, by the optimization algorithm

$$x_i^k = x_i^0 + \Delta x_i^k(\mathbf{x}^0),$$

$$\Delta x_i^k = \Theta_{ig}(\mathbf{x}^0)P_g.$$

The global parametrization is more convenient for global optimization algorithms since they require information about previous steps (during updates or line searches, for instance), and in the case of a Hessian update method. The incremental parametrization gives more flexibility since it only regards the last step in order to construct a new field,

besides breaking the limitations of the initial configuration. The latter strategy is adopted here.

There are two main ways to define the variation field. On one side, it can be defined from the nodal values and interpolated using the same spatial base functions as the numerical method, $\delta\mathbf{x} = \sum \delta\mathbf{x}^i \phi^i$. Alternatively, it can be evaluated at all the requested points, $\delta\mathbf{x} = \delta\mathbf{x}(\mathbf{x})$. The latter method has proved a better response, and is used in the sequel.

### 4.2. Linear deformation field

There is a great freedom in the choice and invention of parametrizations. The most usual ones are based on a definition of the complete geometry by splines of all kinds and orders (in aeronautical shape optimization, usually cubic B-splines, NURBS [25] or Bezier-curves [26]). In identification problems, the geometry is usually defined by simple geometrical entities, in turn defined by a few parameters (like ellipses defined by the coordinates of the center, the axes length and an angle of orientation in [27,28,5]).

A linear variation field is described by a constant deformation tensor (two parameters) plus a displacement of the field (four parameters making a total of six). A definition of more physical meaning, in the sense that it comes from a deformation tensor, is the following:

$$\Theta^6_{ig} = \begin{bmatrix} 1 & 0 & x_2 & x_1 & x_1 & x_2 \\ 0 & 1 & -x_1 & x_2 & -x_2 & x_1 \end{bmatrix},$$

where $\mathbf{x} = \mathbf{x}^{real} - \mathbf{x}^{cg}$ ($\mathbf{x}$ with respect of the centroid of the flaw), $i$ is the index for the direction and $g$ is the index for the parameter, which gives each one a clear sense,

$$P_g = \begin{bmatrix} \delta x_1^{cg} \\ \delta x_2^{cg} \\ \delta\omega \\ \delta\varepsilon_m \\ \delta\varepsilon' \\ \delta\varepsilon_{12} \end{bmatrix} = \begin{bmatrix} \text{first coordinate of the centroid of the flaw} \\ \text{second coordinate of the centroid of the flaw} \\ \text{angle of rotation} \\ \text{spheric strain} \\ \text{horizontal elongation} \\ \text{distortion} \end{bmatrix}.$$

### 4.3. Quadratic deformation field

By expanding the order of the linear variation field up to the second order, we obtain the following base with 12 parameters:

$$\Theta^{12}_{ig} = \begin{bmatrix} 1 & 0 & x_1 & 0 & x_2 & 0 & x_1x_2 & 0 & x_1^2 & 0 & x_2^2 & 0 \\ 0 & 1 & 0 & x_1 & 0 & x_2 & 0 & x_1x_2 & 0 & x_1^2 & 0 & x_2^2 \end{bmatrix}.$$

### 4.4. Numerical evaluation

After substituting the desired parametrization $\delta x_i = \Theta_{ig}\delta P_g$ into the geometrical sensitivity expressions (Eqs. (23)), the following expressions are derived:

$$\delta r_i = (\Theta_{ig}(\xi) - \Theta_{ig}(x))\delta P_g,$$

$$\delta n_i = t_i t_m t_l \varepsilon_{mk} \Theta_{kg,l} \delta P_g,$$

$$\delta S = t_k t_l \Theta_{lg,k} \delta P_g. \tag{16}$$

Substituting Eqs. (16) into (14), the system of sensitivity equations can be written as

$$c^i_k \delta u_k(\boldsymbol{\xi}) + \int_\Gamma [\sigma^i_{jk}(\mathbf{x},\boldsymbol{\xi}) n_j(\mathbf{x}) \delta u_k(\mathbf{x}) - u^i_k(\mathbf{x},\boldsymbol{\xi}) \delta q_k(\mathbf{x})]\, d\Gamma(\mathbf{x}) = {}^g U^i_g(\boldsymbol{\xi}) \delta P_g,$$

$$\begin{aligned} {}^g U^i_g(\boldsymbol{\xi})\delta P_g = &- \int_\Gamma [(\sigma^i_{jk,m}(\mathbf{x},\boldsymbol{\xi}) n_j(\mathbf{x}) u_k(\mathbf{x}) - u^i_{k,m}(\mathbf{x},\boldsymbol{\xi}) q_k)\delta r_m(\mathbf{x},\boldsymbol{\xi}) \\ &+ (\sigma^i_{jk}(\mathbf{x},\boldsymbol{\xi}) n_j(\mathbf{x}) u_k(\mathbf{x}) - u^i_k(\mathbf{x},\boldsymbol{\xi}) q_k)\delta S(\mathbf{x}) \\ &+ \sigma^i_{jk}(\mathbf{x},\boldsymbol{\xi}) u_k(\mathbf{x}) \delta n_j(\mathbf{x})]\, d\Gamma(\mathbf{x}). \end{aligned} \tag{17}$$

The discretization of the variation BIE (17), yields the following expression in matricial form:

$$\mathbf{H}\delta\mathbf{u} - \mathbf{G}\delta\mathbf{q} = \boldsymbol{\Delta}\delta\mathbf{P}, \quad \boldsymbol{\Delta} = {}^g U^i_g(\xi),$$

where $\delta\mathbf{u}$ and $\delta\mathbf{q}$ are the displacement and stress variation vectors and $\delta\mathbf{P}$ is the parameter set variation. $\mathbf{H}$ and $\mathbf{G}$ are identical to the system matrices in the forward problem. $\boldsymbol{\Delta}$ is a matrix that groups the rest of the integrals.

The application of the boundary conditions yields the same coefficients of the system matrix $\mathbf{A}$ as the forward problem, since the prescribed values have zero variation. These variations are therefore not unknowns, as if they were prescribed:

$$\mathbf{A}\delta\mathbf{v} = \boldsymbol{\Delta}\delta\mathbf{P},$$

where $\delta\mathbf{v}$ groups the non-prescribed terms of $\delta\mathbf{u}$ and $\delta\mathbf{q}$ in the sequel, as done in the BEM. The solutions of the latter system for each column of $\boldsymbol{\Delta}$ can be performed and grouped into $\mathbf{J}$, called jacobian, as

$$\delta\mathbf{v} = \mathbf{J}\delta\mathbf{P} \;\Rightarrow\; \mathbf{J} = \{j_{ig}\} = \left\{\frac{dv_i}{dP_g}\right\}.$$

From a computational point of view, this procedure is cheap since the system matrix $\mathbf{A}$ is already computed and

factorized from the forward problem, so the remaining operations are the sequentia back and forward substitutions of the columns of $\mathbf{\Delta}$.

## 5. The solution of the IP

The used solution strategy for the IP, stated as the computation of the parameters that best adjusts the response prediction from a numerical model to the real measurements, and formulated as a minimization problem of a cost functional $\mathscr{J}$ for the parameters $P_g$ that characterize the defect. For that purpose, a residual vector $\mathbf{R} = \{R_i\}$ is defined to represent the discrepancy in the adjustment.

### 5.1. Residual

We introduce the *residual vector* $\mathbf{R}$ in order to quantify the discrepancy between the measurements and theoretical predictions. While the prediction is based on a set of $g$ parameters $P_g$, the ideal measurement data can be denoted by a corresponding best adjusted set $P_g^r$ where the superscript $r$ denotes real defects:

$$R_i(P_g) = v_i(P_g) - v_i^{ex}, \tag{18}$$

where $v_i$ are the $i$th response to be measured (either displacements or tractions depending on the boundary conditions), first for the computed case $v_i(P_g)$, and second for the experimental measurements $v_i^{ex}$.

### 5.2. Cost functional

A cost functional $\mathscr{J}$ is defined in terms of the former residual $R$ in a quadratic sense, which is also a least squares sense. This definition is meaningful from the statistical point of view, as well as from theory of linear algebra, since is minimizes distances in an Euclidean sense. The cost functional is hence defined as in Eq. (19) for the case of the discrete frequency domain:

$$\mathscr{J} = \tfrac{1}{2}\mathbf{R}^{\mathrm{T}}\overline{\mathbf{R}} = \tfrac{1}{2}\|\mathbf{R}\|^2, \tag{19}$$

where T stands for the transpose in vectorial notation and $\overline{R}$ means the conjugate of the complex magnitude $R$.

### 5.3. Selection of minimization algorithm

An approximate classification of the usual methods for IP solution depending on the scope of the convergence is shown in Fig. 2.

The natural evolution of the currently available mathematical programming methods from the most simple to the most sophisticated ones is exposed here. A good survey on them was carried out by Dennis and Schnabel [29], and others [30,31]. The most promising methods among them were tested in conjunction with the sensitivity supply and BEM for static measurements by Rus and Gallego [32,33]. It was shown that the *Levenberg–Marquardt* method usually coupled a higher convergence speed in terms of iterations with higher probability of success. The latter method has therefore been adopted as the standard in the sequel.

#### 5.3.1. Levenberg–Marquardt and trust region approach (TRA)

By a multivariable Taylor series expansion of any function $f(\mathbf{x})$ until the second term, an affine model of $f(\mathbf{x}) : \Re^n \to \Re$ can be defined as

$$m_c(\mathbf{x}_c + \mathbf{p}) = f(\mathbf{x}_c) + \nabla f(\mathbf{x}_c)^{\mathrm{T}}\mathbf{p} + \tfrac{1}{2}\mathbf{p}^{\mathrm{T}}\nabla^2 f(\mathbf{x}_c)\mathbf{p} + h^{\mathrm{T}}h\varepsilon(\mathbf{p}),$$

where $\nabla_i f = \partial f/\partial x_i$ is the gradient, $\nabla^2_{ij} f = \partial^2 f/\partial x_i \partial x_j$ is the Hessian, which will be symmetric if twice continuous differentiable.

The Levenberg–Marquardt method consists in an iterative algorithm in which from a starting guess $\mathbf{x}_k$ the following sequence is repeated:

(1) $(J_k^{\mathrm{T}}J_k - \mu_k I)\mathbf{s}_k = -J_k^{\mathrm{T}}R_k$ subject to $\|\mathbf{x}_{k+1} - \mathbf{x}_k\|_2 \leqslant \delta_k$,
(2) $\mathbf{x}_{k+1} = \mathbf{x}_k + \mathbf{s}_k$.

This is performed as described above in the Model-Trust region. This improves the behavior of the algorithm for $J$ with not full column rank. A line search can be added on this method, $\mathbf{x}_{k+1} = \mathbf{x}_k + \lambda_k \mathbf{s}_k$.

The Model-Trust Region consists in modifying $H_k$ such that $\mathbf{s}_k \leqslant \delta_c$, i.e. $s_k$ is within the trust radius $\delta_c$. Primarily, the step may be chosen by the "hook" step (by

| Global | Local | Setup |
|---|---|---|
| Techniques for Nonlinear Systems of Equations | | Observation Equations |
| Optimization algorithms (Gauss–Newton, Quasi–Newton, Secant, Least–Squares) | | Minimization of cost functional |
| Linear and Quadratic Programming | | |
| Kalman filter, Proyection filter | | |
| Genetic and Evolutionary Algorithms | | |
| Neural Networks; fuzzy inference | | |
| Random search | | |
| Simmulated Annealing | | |
| Topological Derivative | | Initialization |

Fig. 2. A classification of IP strategies.

$(H_c + \mu I)\mathbf{s}(\mu) = -\nabla f(\mathbf{x}_c)$), or, as in our case, by the double dogleg step, which is the point located at a distance $\delta_c$ of the line joining the Newton solution ($-H^{-1}\nabla f$) with the Cauchy solution ($-\nabla f/\|f\|$). Secondly, the trust region can be reduced by yet another backtracking of $f(\mathbf{x}_+) \leqslant f(\mathbf{x}_c) + \alpha \nabla f(\mathbf{x}_+ - \mathbf{x}_c)$.

#### 5.3.2. Normalization

The normalization means a scaling of the problem in the sense that the units and magnitudes of the different parameters involved in the problem (for example the size of the flaw with respect to the total size, or the combination of displacement and stress measurements) may affect the solution.

Whereas Newton and BFGS methods are unaffected by scaling, the steepest descent and therefore the trust region models are affected. Therefore, the values introduced in the algorithms should previously be modified by a scaling matrix $D_x$ in the form, $\hat{\mathbf{x}} = D_x\mathbf{x}$.

There is a further effect that one should care. Too different magnitudes may also affect the conditioning of the matrices due to the computer precision, not only in the optimization algorithms, but also in the BEM calculations. The solution is similar to above.

#### 5.3.3. Stopping

The stopping criteria is a relevant part of the iterative search algorithm. The properties of different stopping criteria in numerical optimization algorithms are the following. Both of the methods are used simultaneously.

- Step: $|\mathbf{x}_k - \mathbf{x}_{k-1}|/\max\{\mathbf{x}_k, \text{typical } \mathbf{x}\} \leqslant \text{tolerance}$. The drawback of this method is that it may get stuck in local minima (or flat regions).
- Residual: $f \leqslant \text{tolerance}$. The drawback of this method is that it requires the residual to become close to zero.

### 5.4. Equivalence between observation equation and Gauss–Newton method

The so-called sensitivity equation has previously been used directly for the solution of IP through the BEM by several authors [19,34,24,20,23,35,36]. The method consists in writing the integral equation and deriving it with respect to a generic geometry variation through a linearization and limit to the boundary. The resulting integral equations give, after the discretization, the relationships between the variation of the measured displacements and the geometrical parameters (a system of equations called $\delta$BIE in the form $\mathbf{A}(\mathbf{x})\delta\mathbf{v} = \mathbf{\Delta}(\mathbf{x})\delta\mathbf{x} \Rightarrow \mathbf{B}(\mathbf{x})\delta\mathbf{x} = \delta\mathbf{v}$). These data are easily related to the residual $\mathbf{R}$ and the geometrical description $\mathbf{x}$, respectively. The $\delta$BIE can then be used in an iterative process starting from an initial guess of the geometry $\mathbf{x}_0$,

(1) Compute $\mathbf{B}(\mathbf{x}_k)$.
(2) Solve the non-square over-determined system of equations $\mathbf{B}(\mathbf{x}_k)\delta\mathbf{x}_k = \delta\mathbf{v}_k$ by least squares ($\mathbf{B}_k^{\mathrm{T}}\mathbf{B}_k\delta\mathbf{x}_k = \mathbf{B}_k^{\mathrm{T}}\delta\mathbf{v}_k$).
(3) Update the geometry $\mathbf{x}_{k+1} = \mathbf{x}_k + \delta\mathbf{x}_k$.

Now, since $\mathbf{R} = \mathbf{v} - \mathbf{v}^{\exp} \Rightarrow \delta\mathbf{R} = \delta\mathbf{v}$ and calling $J = \partial\mathbf{R}/\partial\mathbf{x} = \partial\mathbf{v}/\partial\mathbf{x} = \delta\mathbf{v}/\delta\mathbf{x} = \mathbf{B}$ for a sufficiently small iteration or within a linearized model, a cost functional $\mathscr{J} = \frac{1}{2}\mathbf{R}^{\mathrm{T}}\overline{\mathbf{R}}$ can be defined. Gauss–Newton's method for this functional reads

(1) $J_k^{\mathrm{T}}J_k\mathbf{s}_k = -J_k^{\mathrm{T}}\mathbf{R}_k$,
(2) $\mathbf{x}_{k+1} = \mathbf{x}_k + \mathbf{s}_k$,

which is exactly the same as the process described above. This is yet another justification of the good behavior of Gauss–Newton's method and unifies two methods formerly classified in different families. This link between the two theories may allow the adaptation of techniques of each one into the other, opening new research lines like use of singular value decomposition of linear observation equations onto minimization algorithms in order to damp higher singular values as a regularization technique (see [37, Chapter 7, 38, Chapter 2]), or application of theory of factor analysis (see [37, Chapter 10]), or application of truncated least squares techniques to the definition of the minimization functional (see [38, Chapter 3]), as well as application of error and probability theories to minimization theories, preconditioning, etc.

## 6. Search convergence tests

A set of benchmark problems is used for the complete solution of an IIP using a least squares minimization algorithm: the Levenberg–Marquardt method with line search and gradient supply. The starting configuration or initial guess is the corresponding to Fig. 3 as well as the sought or real configuration. The initial cavities

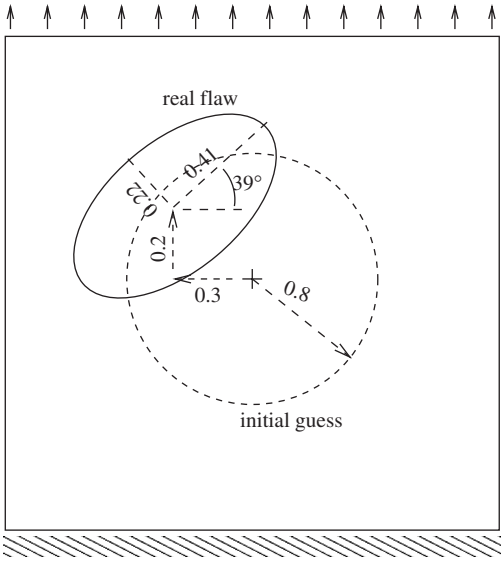


Fig. 3. Description of initial guess for the cavity and inclusion benchmark models.

and inclusions are defined as a centered circle of radius 0.8, and the final ones are ellipses of center $(-0.3, 0.2)$ and semi-axes 0.41 and 0.22, at an angle of $39^\circ$ with the horizontal (like the ones used for the sensitivity tests). The geometry, mechanical properties and numerical treatment is identical to the previous section, excepting the particular refinements tested in each of the following cases.

The identification is made increasing gradually the number of parameters. This is done in four restarts of the optimization algorithm, using the parameters listed in the legend of each problem. The maximum number of iterations per restart is limited to 20, and the maximum increment in the value of each parameter is restricted to 0.2 in order to limit possible divergences. The stopping criteria is $\Delta P = 0.001$.

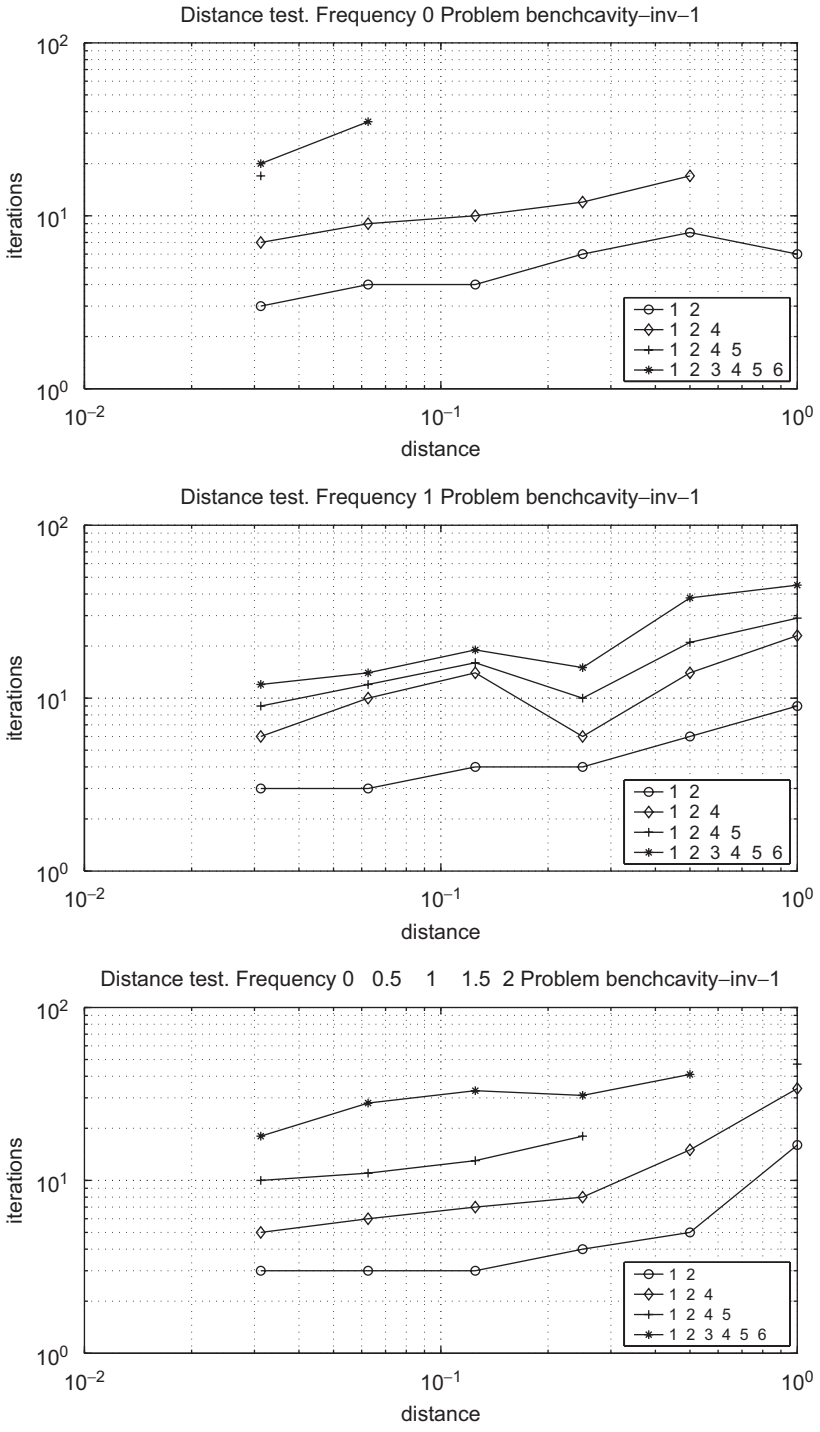


Fig. 4. Convergence versus distance from real flaw. Cavity model. Legend: the different plots correspond to a choice of parameter vector containing a different number of parameters, labelled as the subset of the full parameter vector defined in Section 4.2.

Three plots are made for each benchmark problem: one corresponding to the search with static data; one corresponding to the values at the normalized frequency $\omega = 1.0$, and a third graphic with simultaneous data measured at a set of frequencies $\omega = \{0.0, 0.5, 1.0, 1.5, 2.0\}$, which implies that the input data is five times richer.

### 6.1. Scope of convergence of the search

In order to check the scope of convergence for each model and at each set of frequencies, the number of iterations needed for convergence is plotted versus the relative distance of the initial guess to the real flaw. The

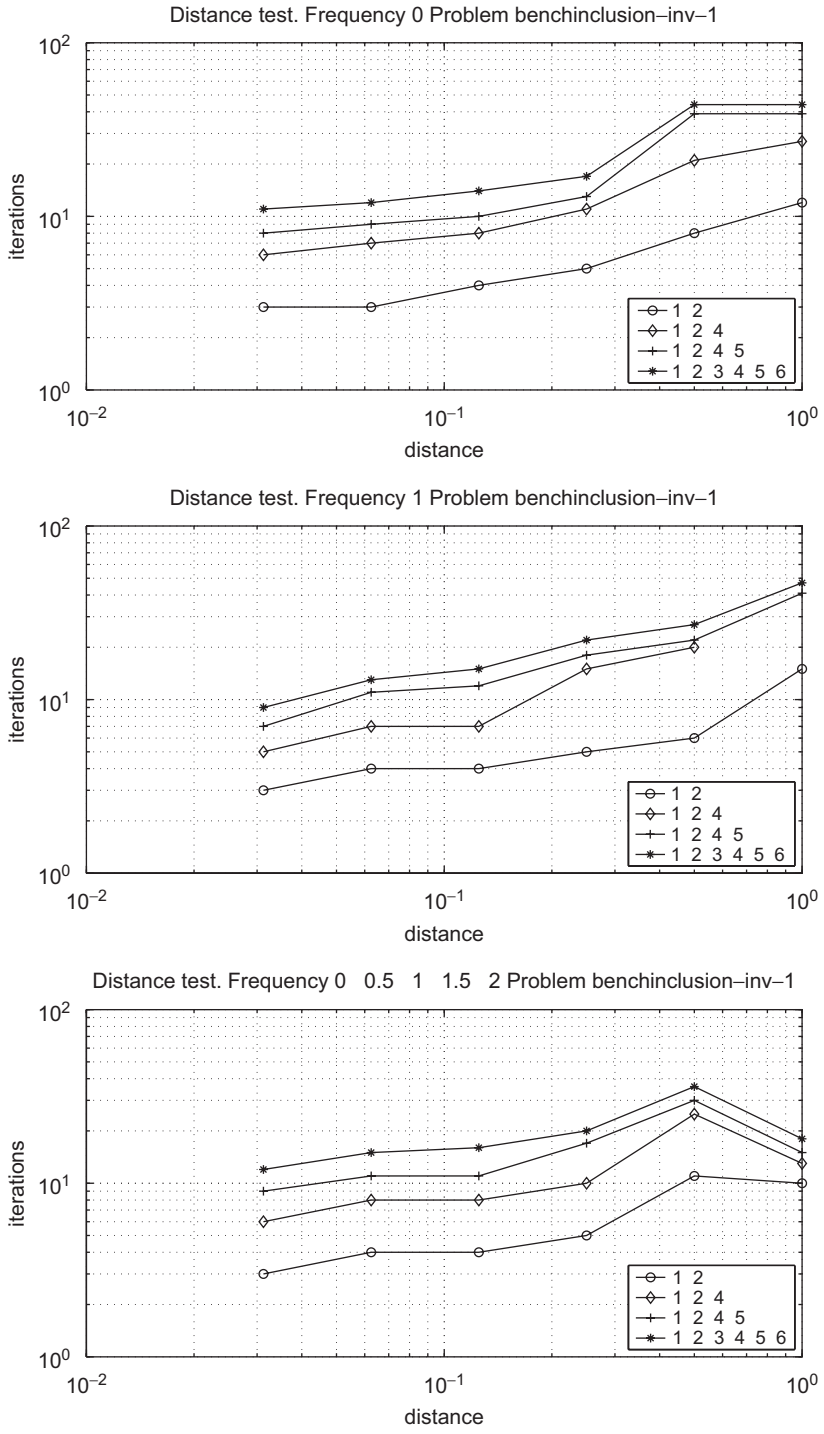


Fig. 5. Convergence versus distance from real flaw. Inclusion model.

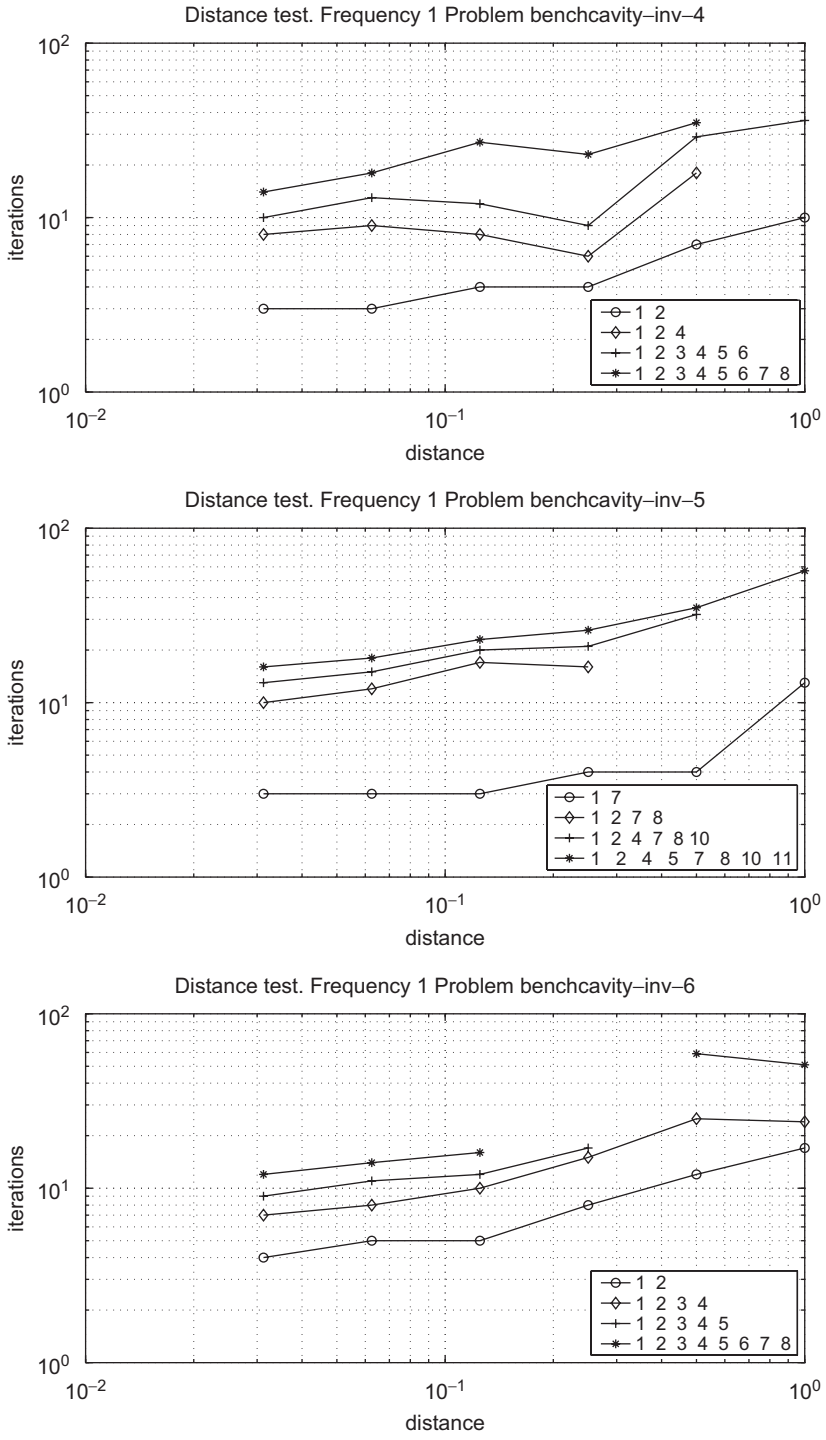


Fig. 6. Convergence versus distance from real flaw. Cavity model with quadratic parametrization.

case of lack of convergence is also represented by a blank in the plot. Figs. 4–6 show the number of iterations needed for the convergence when placing the initial guess at a proportional value between those of the real value and the initial guess. In the case of absence of convergence, the corresponding point is blank. It should be noted that the convergence is not necessarily to the real result, which would give a false identification. The partial results at each restart are plotted. The different lines correspond to a choice of parameter vector containing a different number of parameters, labelled as the subset of the full parameter vector defined in Section 4.2.

From these figures, the necessary iterations increase more or less gradually with the distance and consequent difficulty

of the search. A faster and more stable convergence is shown in the case of inclusions. Complicated parametrizations show some problems at the last parameters.

It is also observed that, as expected, the success in a particular restart is critical for the success of the following one. This justifies the used dosage strategy of parameters.

### 6.2. Convergence with more measurements

The number of data supplied for an IP is an important factor. The problems are now solved acquiring an increasing number of measurements, from a minimum of 8 (all the nodal values on the half right vertical side), and increasing anti-clock-wise along the external boundary until 64 (Fig. 7).

The graphics are all made for frequency $\omega = 1.0$, and for each benchmark problem. The starting guess is placed at an equivalent distance of 0.2. An increasing number of parameters is also shown at every graphic. The number of measurements does not seem to imply important effects in the process of convergence. It should be noted that, unless special regularization techniques are used, the number of measurement data should be equal or higher than the number of parameters in order to allow for the convergence to a realistic solution.

### 6.3. Simulated errors

In order to simulate real cases, some errors are introduced in all parts of the model: measurements, geometry (alteration of the coordinates of each node), elastic modulus, other elastic constants, and frequency. The errors are defined by a normal distribution of zero mean and variance defined by the percentage of error. Figs. 8–10 show the final value of the geometrical invariants error (area, center of gravity, and the 2D moments of inertia) when a particular error amplitude is simulated on the measurements, geometry, elastic modulus, and other material constants or frequency. The amplitude of variance of the gauss-distributed error is set as 0, 0.005, 0.02, 0.05, 0.10, i.e., up to 10% of the maximum measurement value. The lack of convergence is represented by a blank plot.

These examples show that the fitness of the final estimation is very fast distorted already at small errors, but looking at the values of the error, the estimation may

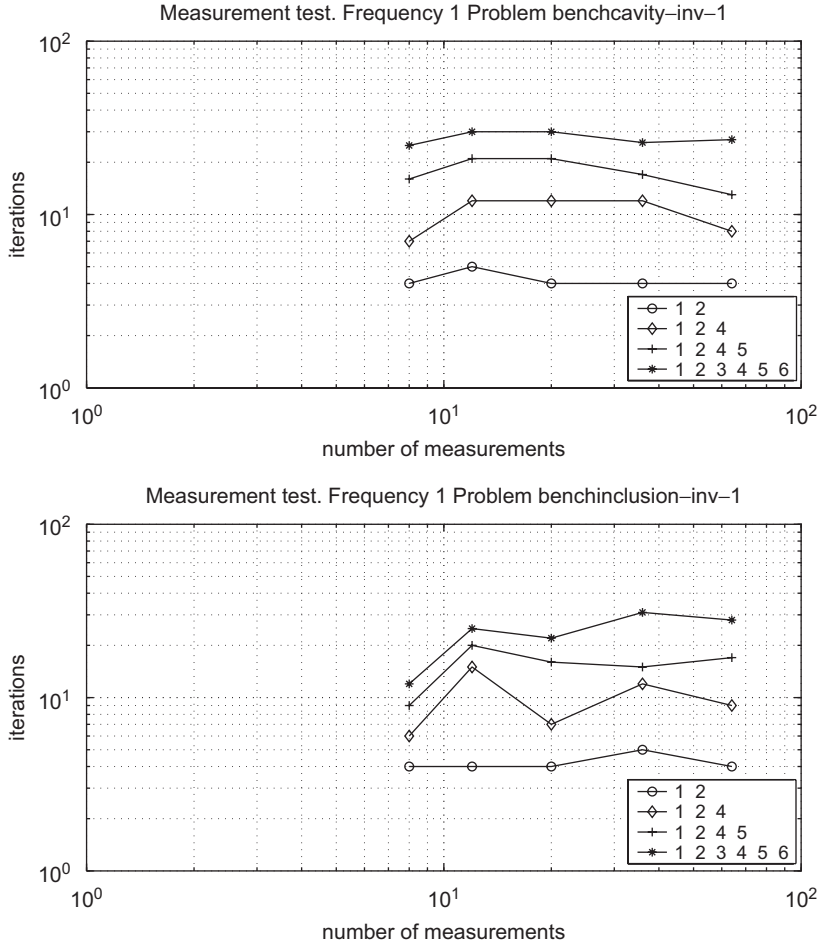


Fig. 7. Convergence with different number of measurements and parameters. Above: cavity model. Below: inclusion model.

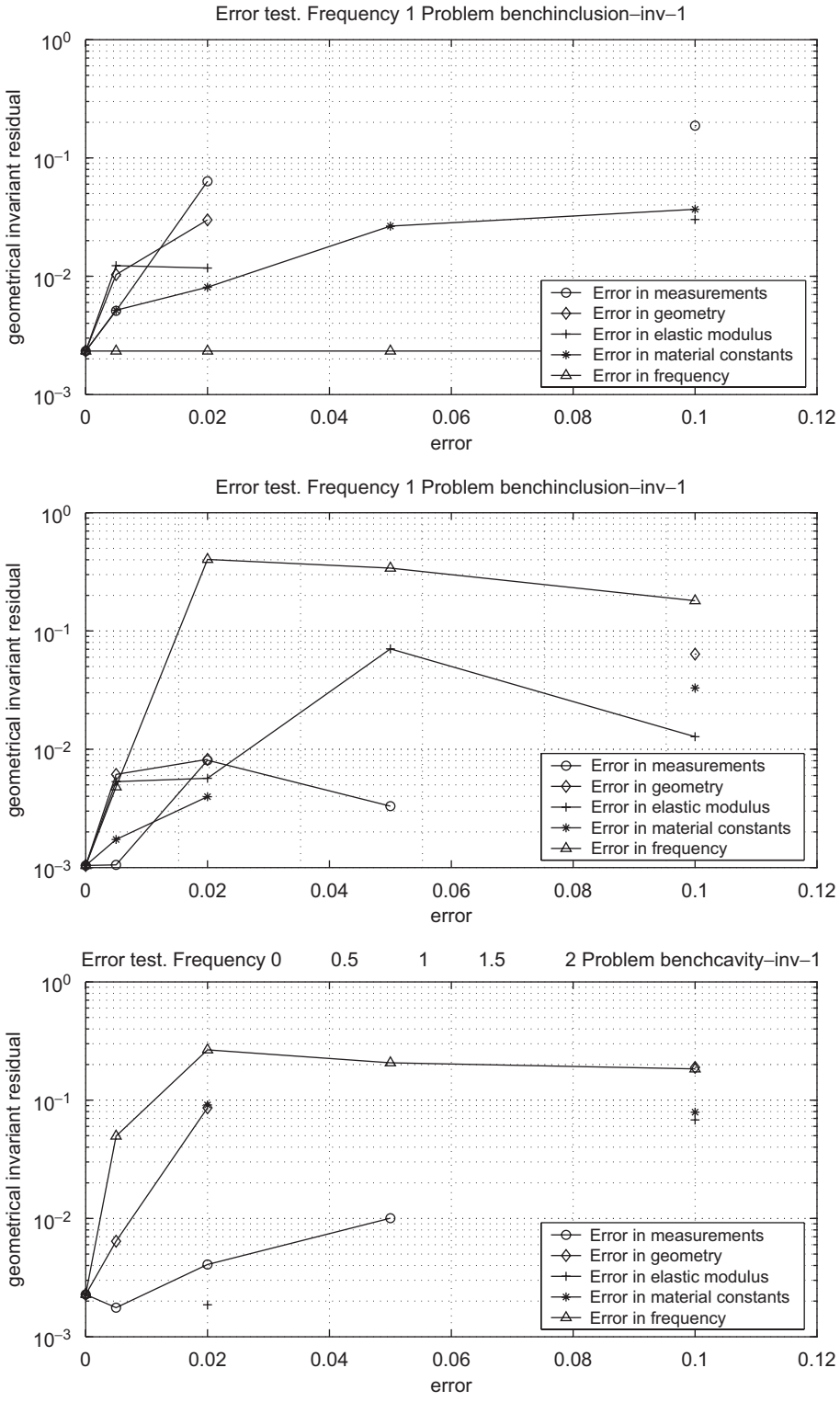


Fig. 8. Convergence with simulated errors. Cavity model.

still be reasonable, taking into account the ill-posedness inherent to identification IPs.

Inclusion problems show a more stable convergence and a higher ratio of success. It is not easy to rank the importance of the error in each part of the model, due to a low correlation between different examples.

### 6.4. Example: detection of a subsurface inclusion

A single problem simulating a soil made of two layers is presented. An flat inclusion in the lower layer is sought by measuring the displacement of a set of five nodes, on the area shown in Fig. 11. The excitation to the body is a

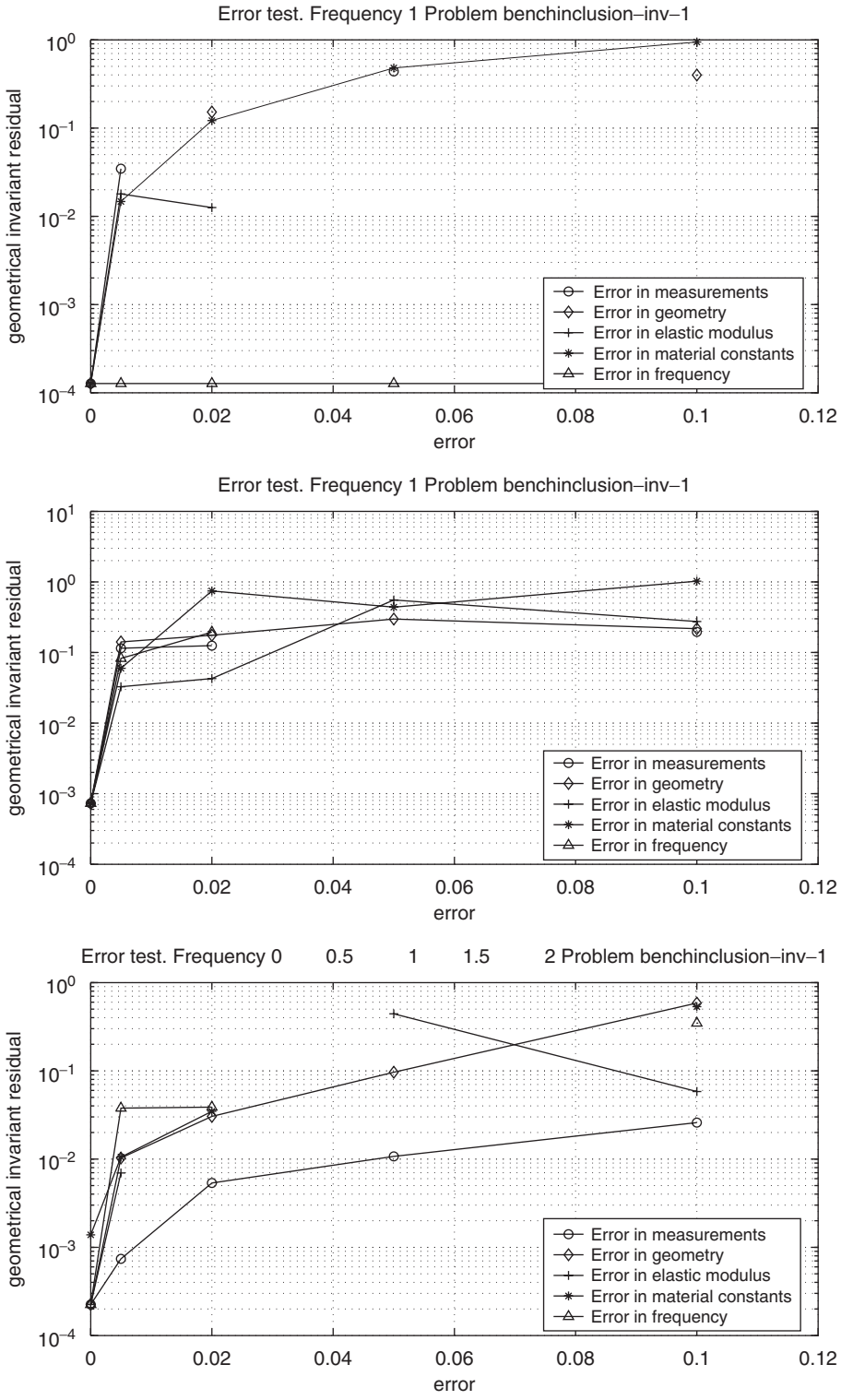


Fig. 9. Convergence with simulated errors. Inclusion model.

parabolic load beside the measurement zone. The mechanical properties of the materials in the different layers and the inclusion are given. In addition, the density is 1.0 and the damping ratio 10% throughout, for frequency $\omega = 1.0$. The model is made of 13 quadratic boundary elements altogether, as specified in Fig. 11.

This may simulate the search of an oil deposit, a drainpipe or an inclusion in piece of cast iron, for instance. Fig. 11 shows the successive geometries during the iterative procedure. The real inclusion is plotted in discontinuous red line, and the final guess is plotted in continuous blue line. The problem mesh is refined to 26

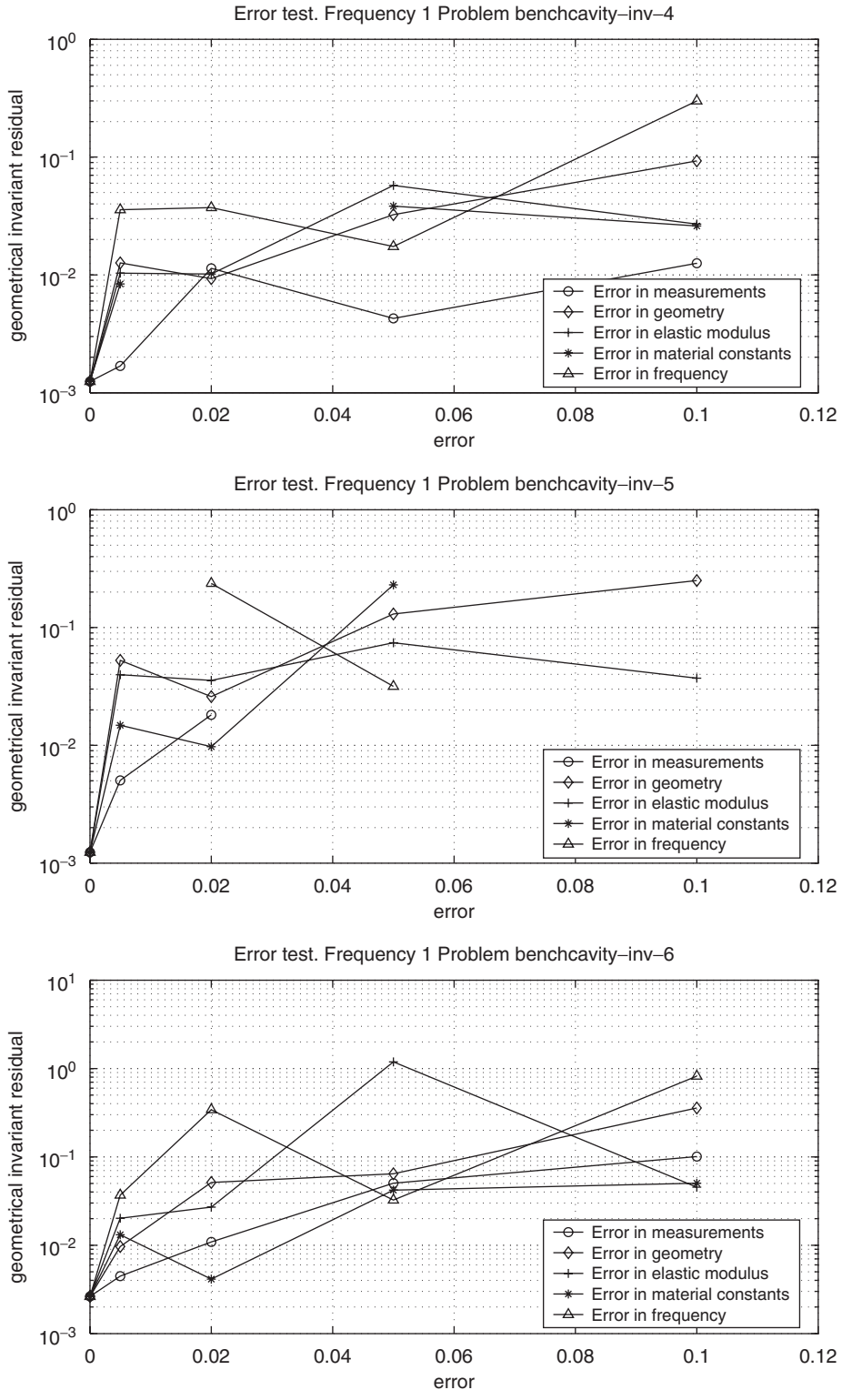


Fig. 10. Convergence with simulated errors. Cavity model with quadratic parametrizations.

elements altogether. The right graphic shows the geometrical error in terms of the square sum of the difference of the geometrical invariants between estimated and real flaws. forty-three iterations are needed to reach a good estimation, and a fast convergence is shown at the beginning. The iterative procedure has been divided in two steps: one allowing only the displacement and radial growth of the circular guess (which converges after 13 iterations), and a second step allowing the flattening too.

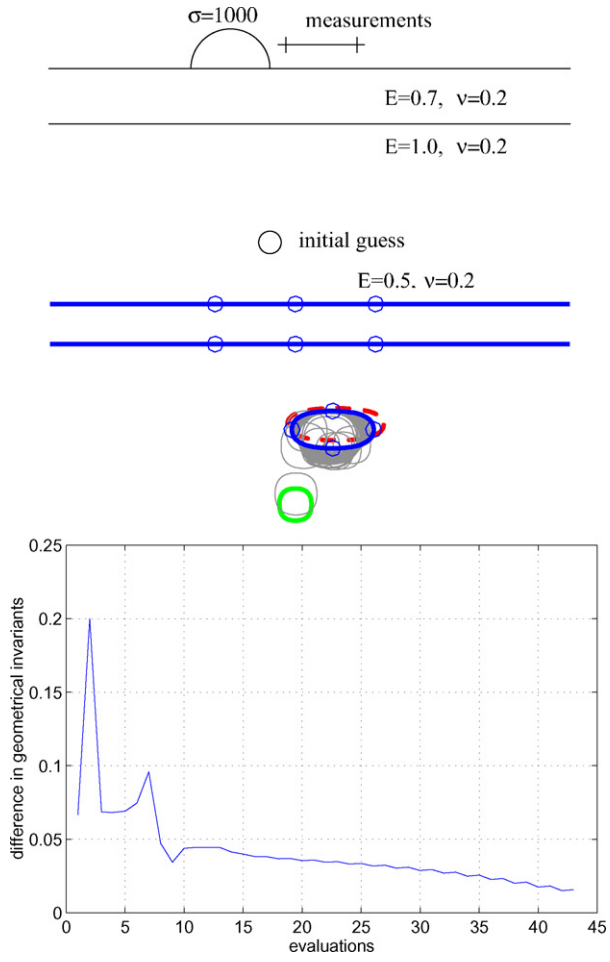


Fig. 11. Model geometry, iterations and geometrical convergence.

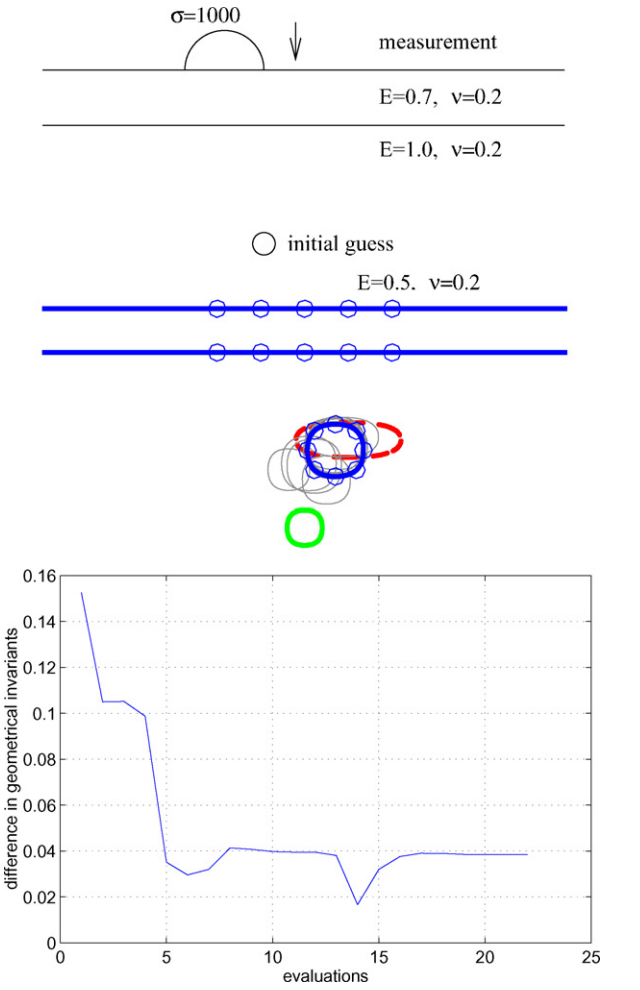


Fig. 12. Model geometry, iterations and geometrical error. Use of waveform analysis.

As a result, the difference in geometrical invariants is represented versus the number of evaluations. The geometrical invariants are just the sum of squares of the difference of first order invariants, which are the coordinates of center of gravity of the inclusion, and the second order invariants, which are the moment of inertia of its geometry.

The same problem is repeated using an unique measurement: the vertical component of the displacement at the point shown in Fig. 12. The data obtained is a sampling of the permanent waveform, which is transformed into its harmonic amplitudes and their phase shift. The first six harmonics are used for the detection, leaving the rest of the definitions as above. Fig. 12 shows the iteration procedure and the geometrical error, as before. The convergence is achieved in $13+11$ iterations, being a somewhat worse solution the cost of a cheap experimental setup with only one transducer.

## 7. Conclusions

A procedure to obtain the gradient or sensitivity of singular boundary integral equations is developed. The sensitivity is obtained analytically before discretization and before parametrization. The latter is moreover defined with respect to a generic differential variation field of the geometry. The conditions required by all the kernels, discretization and parametrization are studied, assuring the applicability. Besides, all the necessary tools for the numerical implementation have been developed and tested.

The numerical values converge perfectly in statics and steady state dynamics, for models with both simple and complex geometries. The convergence of the gradient values while improving the discretization is steady in every example, at similar rates to the solution of the direct problems. This fact together with a visually identical value in comparison with the gradient estimation by finite differences guarantees that the correct values are being obtained.

The finite difference method seems to fail in the low frequency dynamic problems, since a large finite distance amplifies nonlinear effects, whereas small values unstabilize rapidly due to low frequency-related numerical inaccuracies in the direct problem. This inaccuracy together with

the much higher computational cost of finite differences recommends the use of direct differenciation.

The functionality of the sensitivity is confirmed by the application to the solution of complete IPs using the Levenberg–Marquardt search algorithm. The test of convergence has been made including all the possible errors: measurement, model, geometry and frequency, attaining reasonably good results. The scope of convergence has been systematically studied by exploring the range of distances from which the correct solution is reached, in order to show the capabilities and reliability of the method.

Finally, a technique for identification based on the study of the steady state waveform is presented. It simply consists on the harmonic decomposition of the response to a non-sinusoidal harmonic excitation. This permits cheaper measurements at fewer or only one point, and allows for much less computing cost that transient analysis as well as more precision in the measurements. Nonetheless, steady state dynamics is readily extensible to linear transient dynamics by a simple Fourier Transform.

## Appendix. Geometrical variation of the boundary differential and the normal vector

For the derivation of the complete $\delta u$BIE, it is useful to consider the variation of some geometrical quantities that arise in the following sections. To do that, the perturbed domain and any magnitude computed in it is notated with an upper tilde. The variation of the normal and the boundary differential are defined by the equations:

$$\tilde{\mathbf{n}} = \mathbf{n} + \delta\mathbf{n} + \text{h.o.t.}, \tag{20}$$

$$\mathrm{d}\tilde{\Gamma} = (1 + \delta S)\,\mathrm{d}\Gamma + \text{h.o.t.} \tag{21}$$

Taking basic geometrical considerations, it can be proved (see [18]) that the variation terms have the following expressions:

$$\delta\mathbf{n} = \varepsilon_{ij}\delta\xi_{j,k}t_i t_k\mathbf{t}, \tag{22}$$

$$\delta S = \delta\xi_{i,j}t_i t_j, \tag{23}$$

where $\varepsilon_{ij}$ is the permutation tensor and $t_i = \mathrm{d}\xi_i/\mathrm{d}\Gamma$ is the tangent vector to the boundary.

## References


[1] Kubo S. Classification of inverse problems arising in field problems and their treatments. In: Tanaka M, Bui HD, editors. Inverse problems in engineering mechanics; 1992. p. 51–60.

[2] Nishimura N, Kobayashi S. Determination of cracks having arbitrary shapes with the boundary integral equation method. Eng Anal Boundary Elem 1994;15:189–95.

[3] Meric RA. Differential and integral sensitivity formulations and shape optimization by BEM. Eng Anal Boundary Elem 1995;15:181–8.

[4] Aithal R, Saigal S. Shape sensitivity in thermal problems using BEM. Eng Anal Boundary Elem 1995;15:115–20.

[5] Mellings SC, Aliabadi MH. Flaw identification using the boundary element method. Int J Numer Methods Eng 1995;38:399–419.

[6] Lee BY, Kwak BM. Shape optimization of two-dimensional thermoelastic structures using boundary integral equation formulation. Comput Struct 1991;41(4):709–22.

[7] Rus G, Gallego R. Solution of identification inverse problems by sensitivity boundary integral equation. In: Oñate E, Bugeda G, Suárez B, editors. ECCOMAS2000, Barcelona, September 2000.

[8] Mukherjee S, Shi X, Mukherjee YX. Surface variables and their sensitivities in three-dimensional linear elasticity by the boundary contour method. Comput Methods Appl Mech Eng 1999;173:387–402.

[9] Mukherjee S, Shi X, Mukherjee YX. Internal variables and their sensitivities in three-dimensional linear elasticity by the boundary contour method. Comput Methods Appl Mech Eng 2000;187:289–306.

[10] Phan A-V, Mukherjee S. On design sensitivity analysis in linear elasticity by the boundary contour method. Eng Anal Boundary Elem 1999;23:195–9.

[11] Bonnet M. Boundary integral equations and material differentiation applied to the formulation of obstacle inverse problems. Eng Anal Boundary Elem 1995;15:121–36.

[12] Bonnet M. Shape identification using acoustic measurements: a numerical investigation using boundary integral equation and shape differentiation. In: Tanaka M, Bui HD, editors. Inverse problems in engineering mechanics; 1992. p. 191–200.

[13] Bonnet M. A general boundary-only formula for crack shape sensitivity of integral functionals. C R Acad des Sci 1999;327(12):1215–21.

[14] Fata SN, Guzina BB, Bonnet M. Computational basics for elastodynamic cavity identification in a semi-infinite solid. In: Kinnas SA, editor. International association for boundary element methods, UT Austin, TX, USA, 2002.

[15] Bonnet M, Burczyński T, Nowakowski M. Sensitivity analysis for shape perturbation of cavity or internal crack using BIE and adjoint variable approach. Int J Solids Struct 2002;39:2365–85.

[16] Burczyński T, Kane JH, Balakrishna C. Shape design sensitivity analysis via material derivative-adjoint variable technique for 3-D and 2-D curved boundary elements. Int J Numer Methods Eng 1995;38:2839–66.

[17] Guzina B, Fata S, Bonnet M. On the stress-wave imaging of cavities in a semi-infinite solid. Int J Solids Struct 2003;40(6):1505–23.

[18] Rus G. Numerical methods for nondestructive identification of defects. PhD thesis. Universidad de Granada, E.T.S.I. Caminos, C. y P., June 2001.

[19] Tanaka M, Masuda Y. Boundary element method applied to some potential inverse problems. Eng Anal 1989;3(3):138–43.

[20] Gallego R, Suárez J. Solution of inverse problems by boundary integral equations without residual minimization. Int J Solids Struct 1999;37:5629–52.

[21] Rus G, Gallego R. Boundary integral equation for inclusion and cavity shape sensitivity in harmonic elastodynamics. Eng Anal Boundary Elem 2005;25:77–91.

[22] Brebbia CA, Domínguez J. Boundary elements, an introductory course. Southampton: WIT Press, Computational Mechanics Publications; 1992.

[23] Gallego R, Suárez J. Numerical solution of the variation boundary integral equation for inverse problems. Int J Numer Methods Eng 1999;49:501–18.

[24] Suárez FJ. Aplicación del método de los elementos de contorno a la resulución del problema inverso en elastodinámica. PhD thesis, Universidad de Granada, E.T.S.I. Caminos, C. y P., Noviembre 1998.

[25] Altmann A. About nonuniform rational b-splines—nurbs. Worcester Polytechnic Institute, USA, 2002. ⟨www.cs.wpi.edu/matt/cs563/talks/nurbs.html⟩.

[26] Vass GJ. The bezier curve. A pov-ray tutorial, 2002. ⟨www.geocities.com/CapeCanaveral/Launchpad/7394/⟩.

[27] Bezerra LM, Saigal S. A boundary element formulation for the inverse elastostatics problem (iesp) of flaw detection. Int J Numer Methods Eng 1993;36:2189–202.
[28] Yao Z, Gong B. Defect identification using boundary element methods of elastostatics. In: Bui Tea, editor. Inverse problems in engineering mechanics; 1994.
[29] Dennis Jr JE, Schnabel RB. Numerical methods for unconstrained optimization and nonlinear equations. Philadelphia, PA: SIAM; 1996.
[30] Råde L, Westergren B. Mathematics handbook for science and engineering. Berlin: Springer; 1999.
[31] Inc M. Matlab optimization toolbox user's guide, ⟨http://www.mathworks.com⟩, 1996.
[32] Rus G, Gallego R. Optimization algorithms for identification inverse problems with the boundary element method. Eng Anal Boundary Elem 2002;26:315–27.
[33] Rus G, Gallego R. Optimization algorithms for identification inverse problems. In: Oñate BSE, Bugeda G, editors. CMEM2001, 2001.
[34] Zeng X, Saigal S. An inverse formulation with boundary elements. Trans ASME 1992;59:835–40.
[35] Gallego R, Suárez J. Solution of inverse problems by boundary integral equations without residual minimization. Int J Solids Struct 1999;37:5629–52.
[36] Gallego R, Suárez J. Variation boundary integral equation for flaw shape identification. In: Third international conference on inverse problems in engineering: theory and practice; 1999.
[37] Menke W. Geophysical data analysis. Discrete inverse theory. New York: Academic Press; 1984.
[38] Hansen PC. Rank-deficient and discrete ill-posed problems. Numerical aspects of linear inversion. Philadelphia, PA: SIAM; 1997.